DIAGNOSING AND FORECASTING AIRCRAFT TURBULENCE WITH STEEPENING MOUNTAIN WAVES

Donald W. McCann

McCann Aviation Weather Research, Inc.
Overland Park, Kansas

Abstract

If aviation forecasters are to understand why pilots complain of rough rides in some weather situations over mountains, they should understand how mountain waves produce turbulence. Unfortunately, the extensive research in breaking mountain waves has barely reached operational meteorology. This paper summarizes the pertinent theory so that a forecaster can recognize the atmospheric conditions favorable for mountain wave breaking. The theory describes two primary parameters needed for mountain wave analysis. First is a local non-dimensional amplitude number (an inverse Froude number). When this number is greater than one, the wave is nonlinear which indicates wave breaking. Second is the wave drag which estimates the wave energy available for turbulence. These two parameters depend on the vertical distribution of stability and wind, which a forecaster can assess on atmospheric soundings, and the height of the mountain. A new term, "breaking wave drag," is defined as the wave drag of turbulent waves and is a useful metric for diagnosing aircraft turbulence in mountain waves. Breaking wave drag can be computed from the stability and wind vertical profiles when the mountain height is known. Certain atmospheric conditions favor two nonlinear enhancements of mountain waves, hydraulic jump-like phenomena and wave reflection/resonance. In order to forecast breaking wave drag over large areas, the MWAVE algorithm was developed to apply the mountain wave equations to model soundings over high terrain.

1. Introduction

Experienced aircraft pilots know that when they fly over mountainous terrain, they may encounter turbulence caused by mountain waves. Experienced aviation meteorologists know that only pilot reports of turbulence associated with thunderstorms can match the severity of some pilot reports for mountain wave turbulence. Mountain waves are sometimes associated with significant aircraft accidents (Wurtele 1970; Ralph et al. 1997). Research in the early 1950s estimated one mountain wave updraft speed at about 40 m s^{-1} (Blumen 1990) – a speed comparable to vertical motion in severe thunderstorms.

Mountain waves also cause severe downslope winds that have produced major damage in cities such as Boulder, Colorado (Brinkman 1974). Wind gusts greater than 45 m s^{-1} are observed in the stronger downslope wind cases. Again, the severity of some downslope wind events can only be matched by the severity of some thunderstorm events.

Mountain waves develop as air flows over a mountain in a stably stratified atmosphere. Since buoyancy is the restoring force, mountain waves are internal gravity waves. Mountain waves oscillate in the vertical at the Brunt-Väisälä frequency:

$$N = \left(\frac{g}{\Theta} \frac{d\Theta}{dz} \right)^{1/2} \quad (1)$$

where g is gravitational acceleration, Θ is the potential temperature, and dz is the layer thickness. Note that in unstable conditions ($N^2 < 0$) air parcels accelerate away from their original level and no gravity wave develops.

If the wave amplitude is large enough, then the waves become unstable and break. Analogous to breaking water waves, the atmospheric flow becomes turbulent which can affect an aircraft. Most mountain waves probably do not break. Forecasters are familiar with mountain waves seen on satellite imagery in the lee of mountains. Since the wave energy propagates horizontally, these do not break. Even waves with significant vertical propagation do not break unless they encounter special atmospheric conditions. Thus, the forecast problem is determining whether these special atmospheric conditions exist over a mountain.

Numerous investigators have published research articles furthering the understanding of mountain waves, but few have focused on their turbulence-producing potential. As a result, practical turbulence forecast methods are rare. Nevertheless, two efforts appear to have promise. First, high resolution numerical models have been successful in simulating breaking mountain waves (e. g. Doyle et al. 2000). However, the resolution needed to run these models (1 km horizontal and 200 m vertical grid spacing) over large mountainous regions is many years away from operational meteorology. Second, mountain waves transport momentum upward from the mountain, but any turbulence aloft dissipates the mountain wave. This causes the momentum to be deposited onto the general atmospheric flow at that level which slows the wind. Today's numerical forecast models have to parameterize these effects in order to keep from overforecasting the wind speed (McFarlane 1987). Therefore, turbulence is a byproduct of this parameterization. Bacmeister et al. (1994) outlines a dynamically-based algorithm for forecasting mountain wave turbulence based on McFarlane's method.

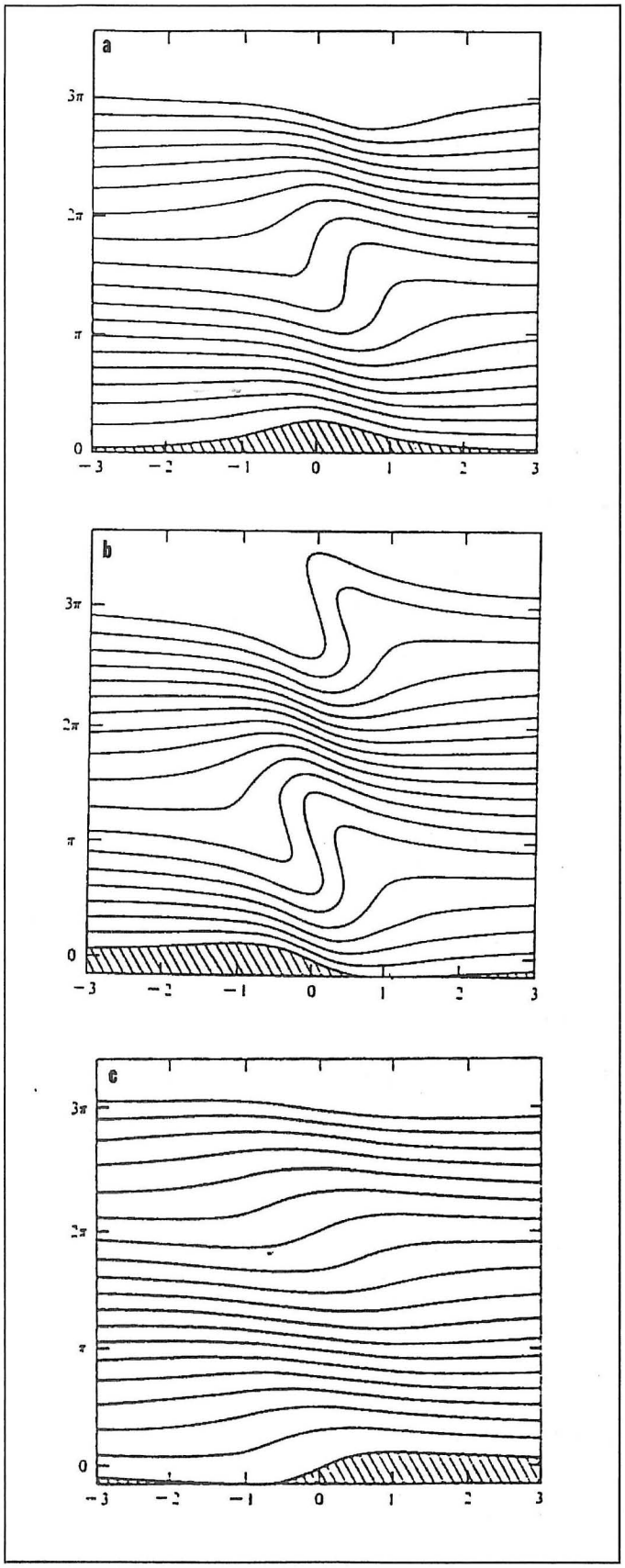

Fig. 1. Numerical solutions to wave equations for varying terrain shapes, a) symmetrical, b) gentle windward/steep leeward slope, and c) steep windward/gentle leeward slope. (From Lilly and Klemp 1979)

The McFarlane/Bacmeister method computes a non-dimensional wave amplitude which is related to wave breaking. By examining the momentum flux or wave energy lost, the method can estimate turbulence intensity. The method works well in the stratosphere where the waves are mostly linear (i.e. the wave fluctuations locally change the atmosphere quickly in comparison with the large scale atmospheric changes). Applying it to the troposphere where most aviation traffic exists sometimes gives unacceptable results because additional nonlinear effects can sometimes create wave turbulence (Laprise 1993)[1].

This paper explains the McFarlane/Bacmeister method in forecaster-friendly terms and shows how a forecaster can subjectively assess the mountain wave turbulence potential on atmospheric soundings. Included are some conditions in which the primary technique fails and ways to apply additional methodology to overcome the failures. The MWAVE algorithm implements the presented formulae to compute aircraft turbulence potential from numerical forecast model grids.

2. The Inverse Froude Number as a Non-dimensional Wave Amplitude

Smith (1979) and Durran (1990) provide excellent source reading for those interested in the general topic of mountain waves. It is not the intent here to provide rigorous mathematical details concerning mountain wave dynamics. The equations introduced in this paper have been derived in the referenced material. These formulae can describe characteristics of breaking waves that are responsible for the turbulence that aircraft encounter (Wurtele et al. 1993).

The basic concepts needed to understand mountain wave phenomena use linear theory of hydrostatic gravity waves as a foundation. This theory is restricted to waves with small amplitudes relative to the background flow. As a first approximation, it has provided qualitative ideas which allow general statements to be made about mountain waves (Smith 1977). Unfortunately, breaking mountain waves are nonlinear. The nonlinear effects control the eventual characteristics of the wave. Although linear theory is not valid for breaking waves, it can be used to diagnose the conditions when wave breaking will occur (Laprise 1993).

A number that measures the nonlinearity of the mountain wave in uniform stability and wind with height is Nh/U, where h is the height of a symmetric mountain from base to peak over which the air flows, and U is the wind speed. This number is a non-dimensional inverse Froude number and will be designated as $\hat{h}$ for convenience. When $\hat{h} > 1$, then the wave becomes nonlinear; it is unstable and breaks (Smith 1977). Turbulence production with mountain waves actually occurs with $\hat{h}$ values lower than one. Miles and Huppert (1969) found that turbulence begins when $\hat{h} > 0.85$, and Smith (1977) derived a wave breaking threshold of 0.74 using second order perturbation theory.

---

[1] Section 6 in this paper discusses two of the most common nonlinear effects.

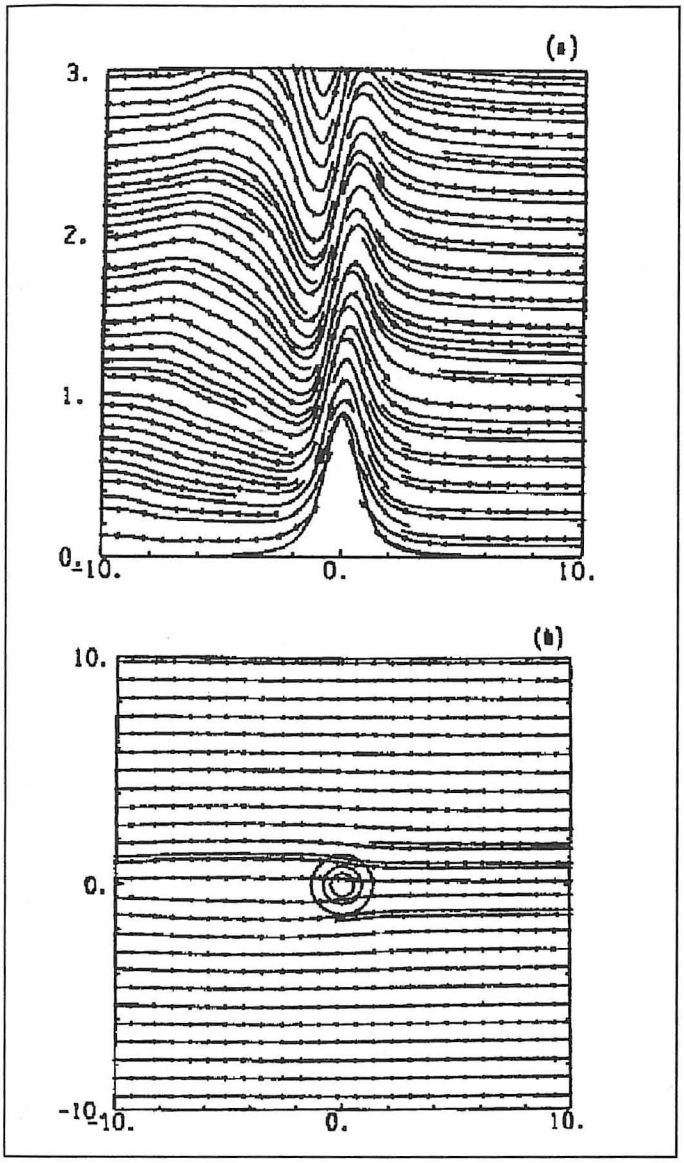

Fig. 2. Numerical simulations of flow past a circular bell-shaped mountain with $Nh/U = .045$. a) Flow in the x-z plane. b) Flow in the x-y plane. (Units in km) (From Smolarkiewitz and Rotunno 1989)

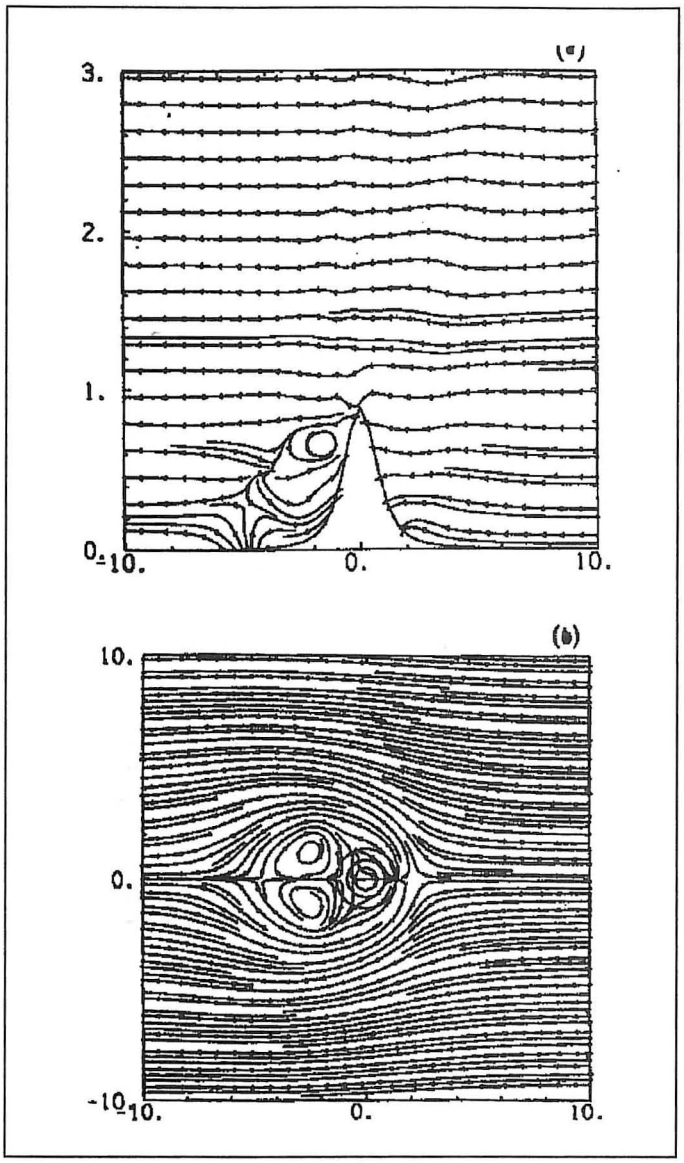

Fig. 3. Same as Fig. 2 except $Nh/U = 4.5$.

Obviously, real atmospheres have variable stabilities and winds with height. Smith (1977) and McFarlane (1987) showed how to account for these variables by calculating a local non-dimensional amplitude number, $\hat{a}$:

$$\hat{a} = \frac{N_z h}{U_z}\left(\frac{N_0 U_0 \rho_0}{N_z U_z \rho_z}\right)^{1/2} \qquad (2)$$

where ρ is the air density, the zero subscripts indicate evaluation at ground level, and the z subscripts indicate the mean evaluation in any layer aloft above sea level. This number, $\hat{a}$, indicates how the initial wave amplitude, $\hat{h}$, changes with height as it propagates upward. Wave breaking thresholds are identical to those of $\hat{h}$, i.e. when $\hat{a}$ is greater than one[2].

Forecasters should take the time to understand the effects of the changes in stability, wind speed, and density with height on wave breaking potential. Layers in which the stability is high and/or the wind speed is low compare more favorably for wave breaking. Breaking potential also increases high in the atmosphere because of the density decrease. Wave breaking is relatively frequent in the stratosphere above mountains because of the high stability, slow winds, and low density. The less frequent occurrences of wave breaking in the troposphere challenge the forecaster.

3. Mountain Height

The non-dimensional amplitude, $\hat{a}$, is also proportional to the mountain height and is assumed to be symmet-

[2] The actual $\hat{a}$ threshold for turbulence depends on the environmental Richardson number. See Appendix A. Turbulence will begin with $\hat{a} > 0.85$ in most instances.

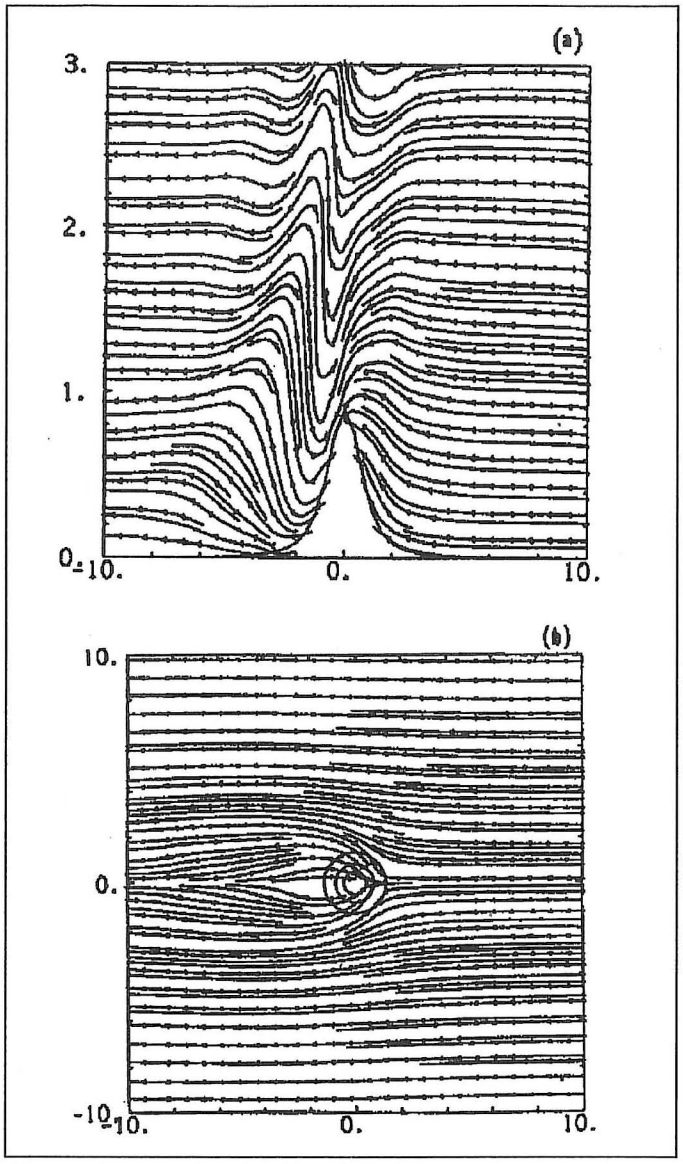

Fig.4. Same as Fig. 2 except $Nh/U = 1.5$

rically-shaped above a flat terrain. The higher the mountain is, the greater the chances for wave breaking aloft. Reality is more complicated because real mountains are not symmetrical, nor is the adjacent terrain flat.

Asymmetry can enhance or diminish a mountain wave (Smith 1977; Lilly and Klemp 1979). Figure 1a from Lilly and Klemp shows a simulated wave that forms from flow over a symmetrical mountain. In Fig. 1b, the lee portion of the mountain is steeper than the windward portion. The wave amplitude that ensues is higher than that for the equally high symmetric mountain. Figure 1c shows a much more shallow wave when the mountain has little downslope steepness. Thus, the downslope steepness is a major influence. Kim and Arakawa (1995) experimented with a number of simple, idealized mountain shapes and confirmed that the downslope steepness has the greatest effect on the wave amplitude.

Intuitively, there exists a symmetric mountain with a height such that the same wave amplitude will occur as over a real mountain. The problem becomes how to estimate this equivalent symmetric mountain height. One simple solution is to look on a topographic chart in the region of interest. The downslope elevation change in the direction of the wind often is a good guess at h. Most mountains have a significant downslope only in one direction, so a forecaster can eliminate many situations whenever the wind direction is unfavorable.

What happens when the stability near the ground is very high and the flow is weak? Then the flow might not be able to go over the mountain. Smolarkiewicz and Rotunno (1989) asked the same question in a three-dimensional numerical simulation of flow past an isolated mountain. In Fig. 2, with low $\hat{h}$ (low stability and/or high wind speed), air parcels flow over the mountain. With high $\hat{h}$, as in Fig. 3, a condition under which one expects that air parcels would have difficulty flowing over the mountain, the air indeed flows around the mountain. The high-$\hat{h}$ flow is similar to two-dimensional potential flow past an obstacle. With moderately high $\hat{h}$ (Fig. 4), part of the flow goes over the mountain, and part flows around. There is an elevation, called the effective height ($h_{eff} \leq h$), below which the wind is stagnated and flows around the mountain, while the wind above flows over that mountain. This blocking effect occurs even if the mountain were infinitely long and perpendicular to the flow so that the flow would be two-dimensional (Smith 1990).

4. Wave Steepening and Breaking

Smith (1977) and McFarlane (1987) showed that determining whether wave steepening will occur in any atmospheric layer above a mountain is a matter of examining the vertical structure of $\hat{a}$. An experienced forecaster will be able to qualitatively estimate $\hat{a}$ from a sounding plot in an analogous manner to thunderstorm potential analysis. Layers with stable lapse rates and slow wind speeds are favorable for wave breaking, but must be analyzed while considering the mountain height. The mountain height is analogous to the lifted parcel. That is, all other factors being equal, the higher the mountain, the larger the wave amplitude, and the more likely wave breaking will occur in a layer with a given lapse rate and wind speed. Computing $\hat{a}$ is more enlightening and is a matter of performing an appropriate sounding analysis much like one would compute convective available potential energy (CAPE).

An atmospheric level at which any gravity wave's horizontal velocity becomes equal to the wind flow is called a "critical level." At a critical level, all of the wave's energy is absorbed so the wave cannot propagate vertically. Instead, the wave energy is converted to turbulence as the wave approaches it (Geller et al. 1975; McFarlane 1987). For a mountain wave, a critical level is whenever $U_z = 0$ since a mountain wave's horizontal velocity is zero – the mountain cannot move. Examining Eq. 2, if $U_z = 0$, the non-dimensional amplitude, $\hat{a}$, becomes infinite. As $U_z \rightarrow 0$, there must be a level at which $\hat{a} > 1$. Therefore, between this level and the critical level, wave breaking is causing turbulence. Above a critical level there is no turbulence because $\hat{a} = 0$.

Even if there were no true critical level in the wind speed profile, any layer in which wave steepening is high enough (U_z small enough) will be a turbulent layer. This is called "wave saturation". When waves saturate, wave energy is converted to turbulence, so wave energy decreases. This will reduce the turbulence in layers aloft if atmospheric conditions remain constant. McFarlane (1987) showed that wave saturation can be parameterized by reducing $\hat{a}$ in layers aloft as visualized in Fig. 5. Starting at the mountain top and working upward, each layer is examined for $\hat{a}_z > \hat{a}_s$, where, initially at the mountain top, $\hat{a}_s = 1$. If $\hat{a}_z > \hat{a}_s$, then $\hat{a}_s = \hat{a}_z$ in the layers aloft. The non-dimensional amplitudes are reduced by dividing by the new $\hat{a}_s$. In Fig. 5, $\hat{a}_z > 1$ beginning at Z_1 and reaches a local maximum at Z_2. For levels above Z_2, $\hat{a}_s = \hat{a}_2$. Between Z_2 and Z_3, $\hat{a}_z / \hat{a}_2 < 1$, so in this layer the wave is not saturated. At Z_3, $\hat{a}_z / \hat{a}_2 > 1$, and the wave breaks once again, but $\hat{a}$ has been attenuated. One can easily see that at a true critical level, $\hat{a}_s = \infty$ and $\hat{a} = 0$ in all layers aloft.

In Eq. 2, U_z is the wind speed *without regard to its direction*. Some have considered only the component of the wind aloft along the low-level wind direction (McFarlane 1987). However, in three-dimensional flow, a mountain wave is refracted horizontally at azimuths different from the original low-level wind direction (Smith 1987). As it is refracted, some of the wave energy is absorbed by the turning wind and is not available for wave breaking (Shutts 1995; Broad 1995). If the wind direction changes by 90 degrees or more, all of the energy is absorbed.

To summarize, mountain waves will steepen or flatten depending on the non-dimensional amplitude, $\hat{a}$. Whenever $\hat{a} > 1$, wave breaking will occur. However, turbulence from wave steepening can occur with a non-dimensional amplitude less than one (see Appendix A). Therefore, in order to analyze a mountain wave's turbulence producing potential in any atmosphere, one must examine a vertical profile of $\hat{a}$, as defined by Eq. 2.

5. Wave Drag

Wave breaking can occur in many atmospheric conditions. However, analysis of wave breaking using $\hat{a}$ only yields a yes/no answer for turbulence. There is no information about the intensity of the wave breaking. In other words, under certain conditions wave breaking may result in very light turbulence, while under other conditions wave breaking may result in severe or extreme turbulence.

One quantity that measures the total mountain wave energy per unit volume is the exchange of momentum between the atmosphere and the mountain (Eliassen and Palm 1960). Hoinka (1985a) showed that, in time, the momentum flux becomes equal to the stress that the mountain exerts on the atmosphere. The stress is measured by the pressure difference between the windward and leeward sides of the mountain along a streamline.[3] This difference is called wave drag. Linear mountain wave drag for a bell-shaped mountain with constant stability (N) and wind (U) aloft, D_L, is given by Miles and Huppert (1969) as

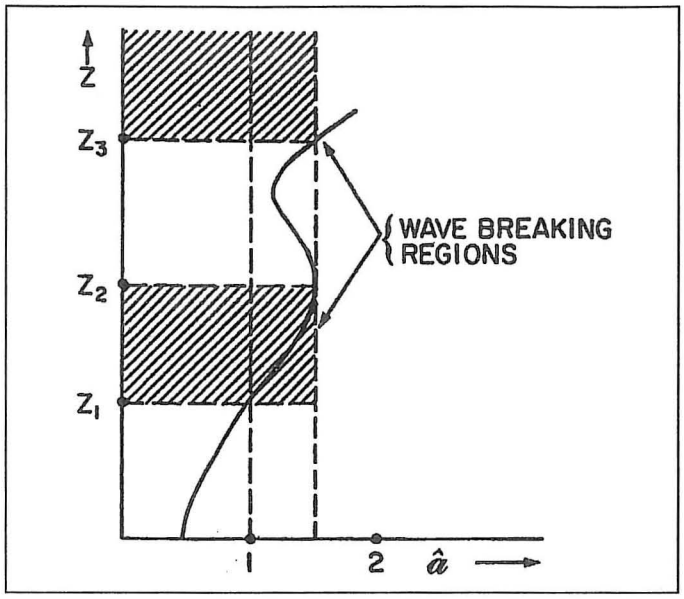

Fig. 5. Schematic vertical structure of the non-dimensional amplitude (â) illustrating layers of wave saturation. (From McFarlane 1987)

$$D_L = -\frac{\pi}{4} h\rho NU \tag{3}$$

This equation yields answers in pressure units. The momentum flux, and therefore the linear wave drag, in any layer aloft is equal to that at the surface through the Eliassen-Palm (1960) theorem assuming no sources or sinks of wave energy exist aloft. This means that D_L in any layer may be evaluated from surface values.

Equation 3 is the formula to compute the linear wave drag of a mountain wave. However, malignant mountain waves that concern aviation are nonlinear. Wave drag of nonlinear mountain waves in numerical simulation models are as much as twenty times the linear value (Peltier and Clark 1979).[4] Miles and Huppert (1969) derived formulae from which nonlinear amplification can be computed. The formula for a bell-shaped mountain is

$$D_{NL} = \left(1 + \frac{7}{16}\hat{a}^2\right) D_L \tag{4}$$

Aircraft often ride a mountain wave's strong up-and-downdrafts with little turbulence. Since the wave drag

[3] At many forecast offices one of the local rules-of-thumb for mountain wave identification is the sea level pressure difference between two stations on opposite sides of the mountain.

[4] The nonlinear amplification of mountain waves computed in numerical models should be taken as ballpark figures since there is some variance from model to model for the same case studies.

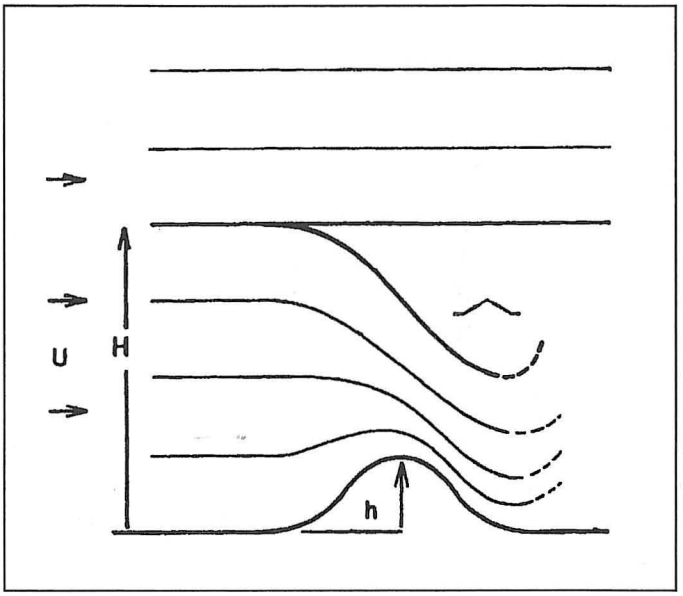

Fig. 6. Schematic diagram of the idealized hydraulic jump-like flow configuration. A critical streamline at level *H* divides with the lower branch descending rapidly. The zone between the split streamlines is turbulent. The streamline recovers back to level *H* in hydraulic jump-like fashion. (Adapted from Smith 1985)

measures the wave's intensity, these observations probably occur when the wave drag is high but the wave steepening potential is low. Therefore, it is the combination of high wave drag and high wave steepening potential that is the serious aviation problem. This paper defines the "breaking wave drag" as the wave drag at levels whenever the wave steepening is large enough to produce turbulence.

6. Nonlinear Enhancements

a. Hydraulic jump-like phenomena

Smith (1985), Durran (1986), Smith and Sun (1987), and Durran and Klemp (1987) have made an analogy of a mountain wave being like an internal hydraulic jump. In shallow water theory, when a more dense fluid is flowing in a channel under a less dense fluid but over an object, if the flow speed and object height are just right, a hydraulic jump at the two-fluid interface will occur. The interested reader in hydraulic jumps can study any fluid mechanics textbook such as Shames (1962).

Durran (1990) explains how this process works in the atmosphere. In the free atmosphere there are no density interfaces such as the water-air interface that typically produce true hydraulic jumps. Nevertheless, an increase in $\hat{a}$ with height can induce hydraulic jump-like behavior in an atmosphere forced to flow over a mountain. Smith's papers (1985, 1987) provide substantial theory for this process. A streamline splits at some level *H* upstream from the mountain with the lower branch descending rapidly (Fig. 6), and the flow becomes much like a hydraulic jump. What level is the level-*H*? It may be a level of high stability (Durran 1986) or a near critical level (Smith 1987). In other words, the level-*H* is where $\hat{a}$ is a maximum.

Turbulence in hydraulic jump-like flow happens in two ways. First, as the dividing streamline descends, the wind speed along the downslope increases as all of the flow below *H* is funneled below the dividing streamline. This increases the wind shear both above and below the speed maximum. Second, the layer between the dividing streamline and the undisturbed flow above it is convectively turbulent, i.e. the potential temperature in the layer locally decreases with height. Smith (1987) observed turbulence below level-*H* to be that which would be expected at level-*H* due to wave breaking.

b. Wave reflection and resonance

Another major nonlinear influence on mountain waves is reflection and the possible resonance interaction of the reflected wave with the original wave. Wave reflection occurs when the refractive index changes rapidly as the wave propagates through it. The refractive index for mountain waves is the Scorer (1949) parameter (N/U in its simplest form). Note that the simple Scorer parameter is roughly proportional to $\hat{a}$ by h. Wave resonance happens when the reflected wave constructively interferes with the original wave, creating a standing wave of greater amplitude. This occurs when the level of refractive index is three-fourths the mountain vertical wavelength (and at $[n+.75]\lambda$, n = 1,2,3,...) (Peltier and Clark 1979). The vertical wavelength can be computed simply by $\lambda = 2\pi U_0/N_0$. Notice that λ does not depend on the mountain height.

If $\hat{a}_{up}$ is the local non-dimensional amplitude of the upward-propagating wave from Eq. 2 and $\hat{a}_{down} = r\,\hat{a}_{up}$, where r is the fraction of the upward wave amplitude reflection downward from the optimum level (0.75λ)[5], then $\hat{a}_{refl} = \hat{a}_{up} + \hat{a}_{down}$. Waves constructively interfere with each other to create wave steepening greater than either $\hat{a}_{up}$ or $\hat{a}_{down}$.

7. Examples

Figure 7a shows a sounding from Lander, Wyoming, at 0000 UTC 4 November 1993. The mountains of concern are the Bighorns in north central Wyoming, about 200 km to the northeast. These mountains are very symmetrical along roughly a north-south axis. From topographic maps, the average height, h, above the surrounding flat terrain is about 1150 m. In Fig. 7b notice the sharp increase in stability above 200 mb with an accompanying decrease in wind speed. For this profile (Fig. 7c) $\hat{a}$ remains well below 0.85 until it rapidly increases to greater than that value above 200 mb. The mountain wave generated at the mountain top near 700 mb would not be turbulent until above 200 mb. This case was chosen because of an aircraft report of moderate to severe turbulence at 41,000 feet (FL410), about 180 mb, that occurred about 3 hours earlier than when this sounding was taken.

The next example in Fig. 8 illustrates that wind decreases with height can also increase $\hat{a}$ to breaking values. The sounding was taken at San Diego, California, on

[5] See Appendix B on how to compute r.

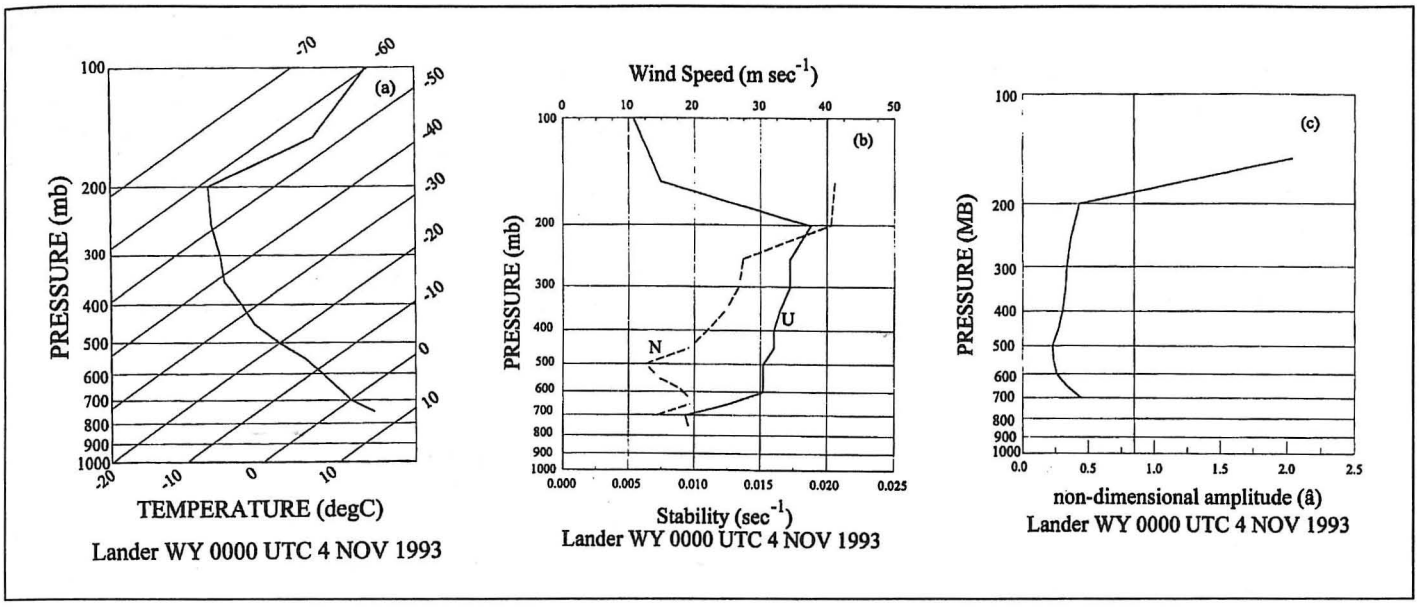

Fig. 7. Wave steepening analysis for the 0000 UTC 4 November 1993, Lander, Wyoming, sounding. a) The skew-T/log-p diagram. b) profiles of wind speed, U (solid) and stability, *N* (dashed). c) Profile of the local non-dimensional amplitude, $\hat{a}$. The vertical line is $\hat{a} = 0.85$.

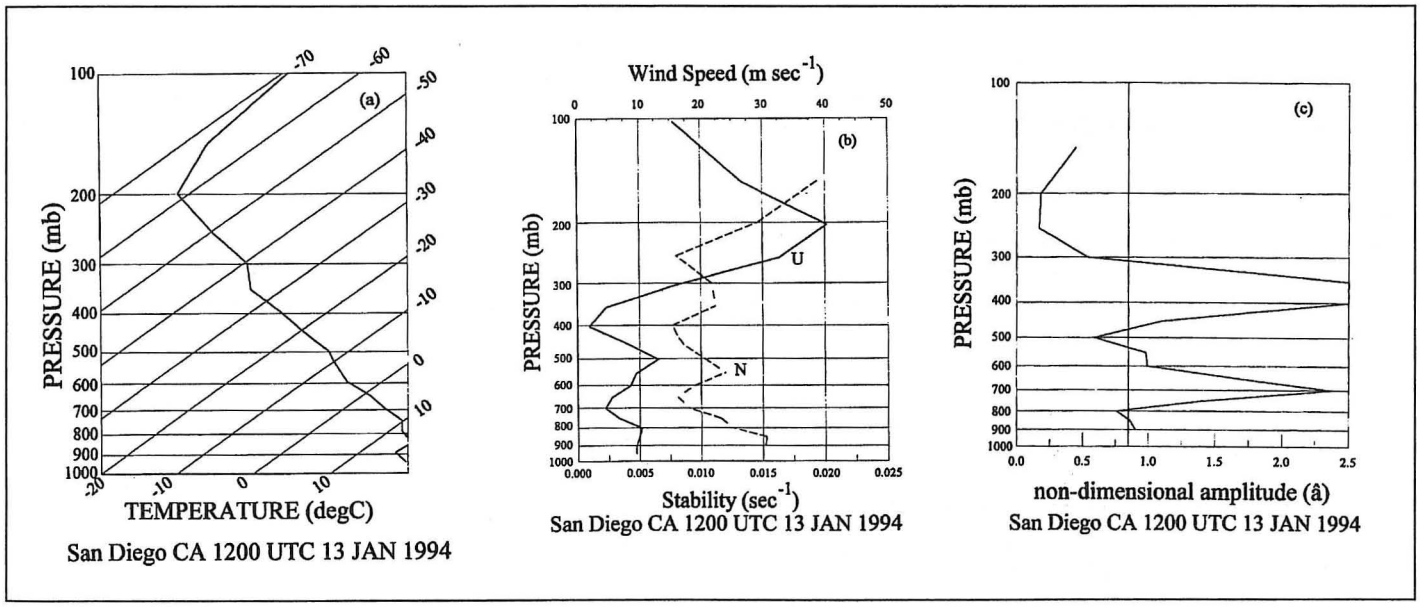

Fig. 8. Same as Fig. 7 for the 1200 UTC 13 January 1994, San Diego, California, sounding.

1200 UTC 13 January 1994. The height of the mountain located 75 km northeast of San Diego is 575 m. This sounding shows wind speeds decreasing to less than 5 m s^{-1} at 700 mb and to near zero at 400 mb. The 400 mb level is almost a critical level. Light turbulence was reported at 700 mb and below.

Figure 9 shows an example of where hydraulic jump-like enhancement probably occurred. The case is of a bora, a downslope wind typical in Croatia, on 6 March 1982 from Smith (1987). The mountain height is 900 m. The higher stability and decreasing winds at 700 mb combined to maximize $\hat{a}$ at that level, and if all $\hat{a}$ at levels below 700 mb are adjusted upward to the maximum $\hat{a}$ (Fig. 9c), then the $\hat{a}$-analysis would correspond to the measured moderate turbulence at all levels below 700 mb (Smith 1987). Not considering hydraulic jump-like phenomena only yields turbulence at 700 mb.

The 11 January 1972 northern Colorado Front Range mountain wave is a good example of reflection/resonance. Figure 10 shows the data for this case. The mountain height was 1900 m. The three-quarter wavelength height (9609 m AGL) was about 160 mb where wave breaking was taking place, and $\hat{a}_{up}(160) = 2.082$. Applying formulae detailed in Appendix B, at the half wavelength level (260 mb), $\hat{a}_{up}(260) = 0.601$. Therefore, $r = \hat{a}_{up}(260)/\hat{a}_{up}(160) = 0.304$ and $\hat{a}_{down} = r\hat{a}_{up}(160) = 0.634$. At 200 mb, $\hat{a}_{up}(200) = 0.89$, so $\hat{a}_{refl}(200) = (\hat{a}_{down} + \hat{a}_{up}\,[200]) = 1.524$. Continuing downward, adding the reflected wave non-dimensional

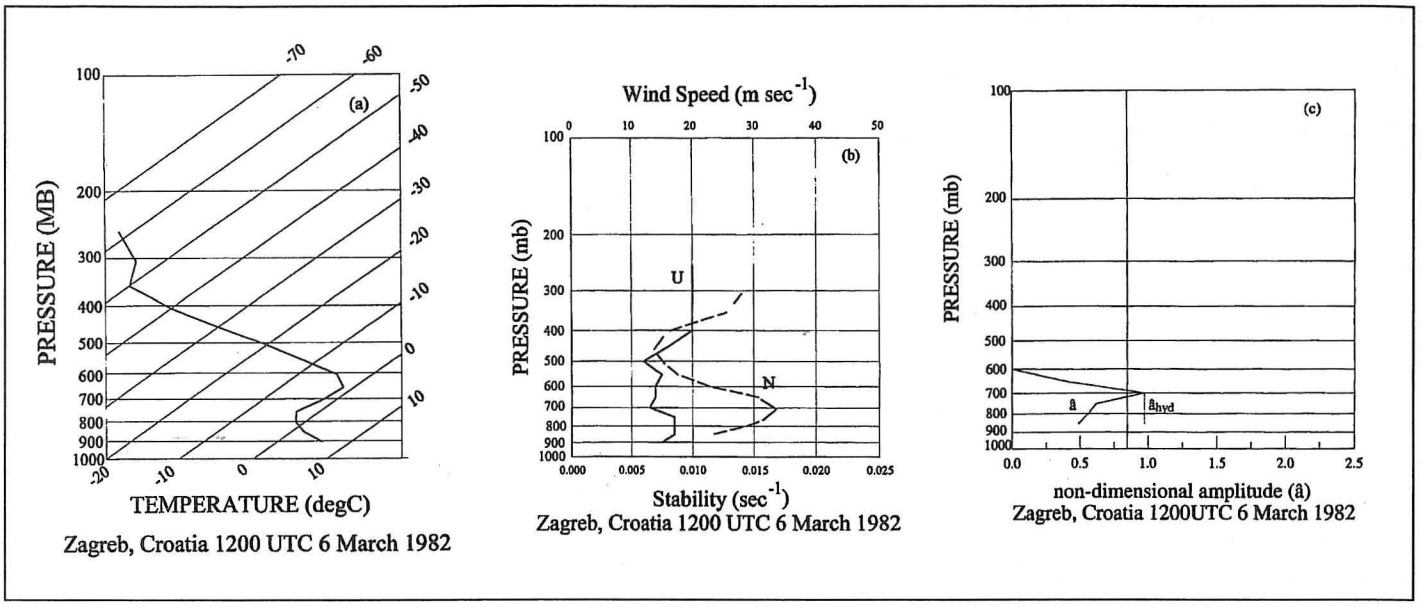

Fig. 9. Same as Fig. 7 for the 1200 UTC 6 March 1982, Zagreb, Croatia, sounding. In c) the dashed line ($\hat{a}_{hyd}$) indicates the non-dimensional amplitude after enhancement for hydraulic jump-like behavior.

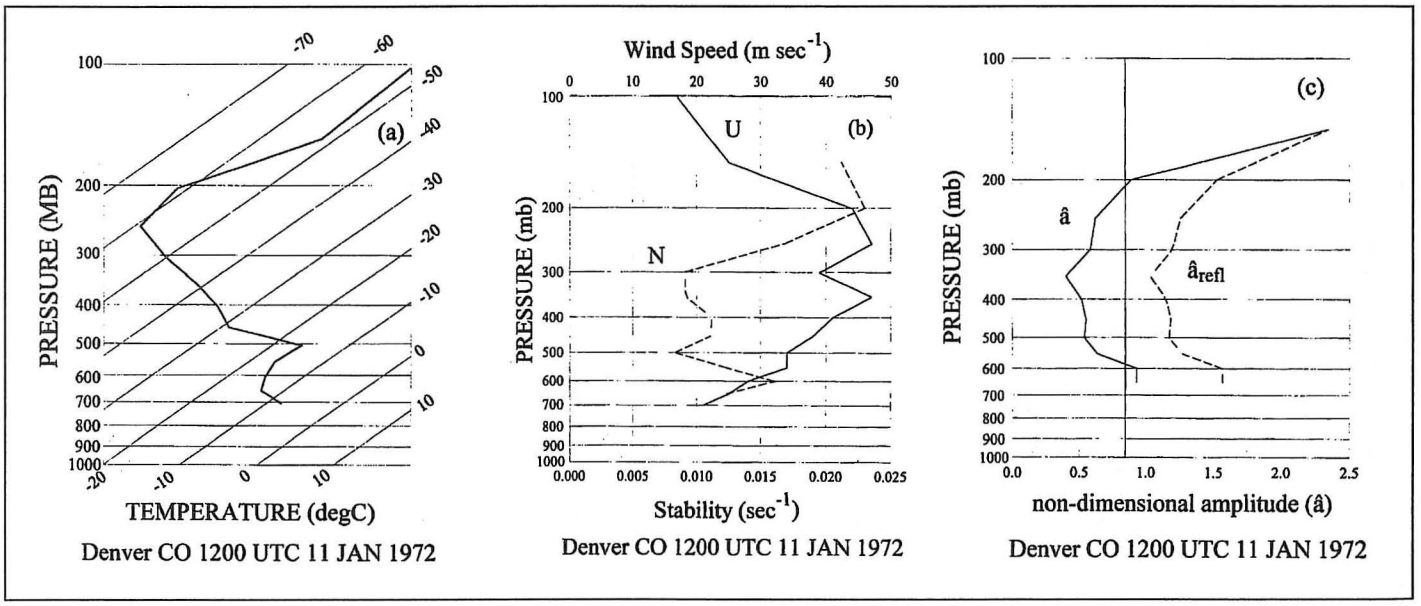

Fig.10. Same as Fig. 7 for the 1200 UTC 11 January 1972, Denver, Colorado, sounding. In c) the dashed line ($\hat{a}_{refl}$) indicates the non-dimensional amplitude after enhancement for reflection/resonance.

amplitude changes the wave analysis at all levels from non-breaking to breaking. This mountain wave is famous not only for its strength but also because it was well observed by research aircraft (Lilly 1978). The aircraft encountered severe turbulence at every level within the mountain wave. Because of the "tuned" atmosphere, reflection/resonance caused a mountain wave that naturally breaks in the stratosphere to also break at lower levels. By not considering this nonlinear enhancement, the turbulence would have been badly diagnosed. These special conditions appear to be rare. In a database of 17 mountain wave cases described in the next section (Table 1), only two were tuned, and only this one shows this magnitude of strength.

These examples show that aircraft turbulence is indeed associated with wave breaking. As noted in Section 5, it is the breaking wave drag that should give the turbulence intensity. Figure 11 shows the breaking wave drag profiles for each of the above examples, and the following section details the breaking wave drag/turbulence intensity relationship.

8. Validation

Breaking wave drag values computed with the formulae outlined above were validated in two databases. First, one hundred aircraft estimates of turbulence intensity at various altitudes for 17 different mountain waves were compared with breaking wave drag computations at

Table 1. List of mountain wave cases used to validate the mountain wave breaking wave drag computations with turbulence from pilot reports. Research aircraft, as documented in the referenced papers, observed the turbulence in the first nine cases. Eight additional cases of known or suspected mountain waves with routine pilot reports supplement the database.

17 February 1970	Lilly and Kennedy (1973)
11 January 1972	Lilly (1978)
6 March 1982	Smith (1987)
7 March 1982	Smith (1987)
22 March 1982	Smith (1987)
23 March 1982	Hoinka (1984)
25 March 1982	Smith (1987)
15 April 1982	Smith (1987)
8 November 1982	Hoinka (1985b)
3 November 1993	north central Wyoming
2 December 1993	south Wyoming/north Colorado
3 December 1993	near Phoenix, Arizona
3 December 1993	near Burlington, Vermont
15 December 1993	near Las Vegas, Nevada
13 January 1994	near San Diego, California
24 February 1994	near Denver, Colorado
27 October 1996	near Tahoe Valley, California

Table 2. A 6 x 5 contingency table of turbulence intensity reports with ranges of breaking wave drag from the Table 1 cases. The Chi-squared test statistic for this table is 136.02 which compares with 45.32 at the .999 level with 20 degrees of freedom.

	Breaking Wave Drag (mb)					
Intensity	**0.0**	**0.0-2.0**	**2.0-4.0**	**4.0-6.0**	**> 6.0**	**Total**
Smooth	17	5	0	0	0	22
Light	7	16	1	0	0	24
Light-Moderate	2	11	1	1	0	15
Moderate	2	8	2	1	0	13
Moderate-Severe	0	2	4	5	0	11
Severe	0	0	1	4	10	15
Total	28	42	9	11	10	100

those altitudes. Table 1 lists the cases. Research aircraft observed the first nine of the waves, and eight additional known or suspected waves with routine pilot reports supplement the database. These seventeen cases represent the entire spectrum of wave intensities ranging from very light to very strong.

The maximum reported turbulence intensity at each 50 mb pressure level within 6 hours of the sounding time were arranged in a 6 x 5 contingency table with ranges of breaking wave drag computed from nearby soundings (Table 2). Only one wave had turbulence reported at all levels. More typical is turbulence

Table 3. Critical Success Indices for breaking wave drag computed from Table 1 cases with variant thresholds for turbulence intensity. Underlined is the maximum for each turbulence intensity. To interpret the table, whenever the breaking wave drag is greater than the underlined threshold, the expected turbulence intensity is at least as high as the column-labeled intensity.

Wave drag (mb)	Light	Lgt-Mod	Moderate	Mod-Sev	Severe
0.0	.807	.671			
0.5	.735	.635			
1.0	.725	.652	.447		
1.5		.589	.516		
2.0		.518	.614		
2.5			.591	.719	
3.0			.545	.766	
3.5				.750	
4.0				.679	.636
4.5					.667
5.0					.722
5.5					.706
6.0					.667

Table 4. Aircraft turbulence report intensities gathered from 7 December 1997 to 6 February 1998 located within 2 degrees of 40N 106W (near Denver, Colorado) and 34N 118W (near Los Angeles, California) compared with the breaking wave drag computed from soundings interpolated from the Rapid Update Cycle numerical model using the MWAVE algorithm. POD is the Probability of Detection and FAR is the False Alarm Rate at the breaking wave drag thresholds recommended in Table 3.

DENVER			
breaking wave drag (mb)	0	>0	
SMOOTH	97	19	POD = 97/233 = .42
> SMOOTH	136	172	FAR = 19/116 = .16
breaking wave drag (mb)	< 2	≥2	
< MODERATE	228	11	POD = 27/185 = .15
≥MODERATE	158	27	FAR = 11/38 = .29
LOS ANGELES			
breaking wave drag (mb)	0	>0	
SMOOTH	63	5	POD = 63/146 = .43
> SMOOTH	83	76	FAR = 5/68 = .07
breaking wave drag (mb)	< 2	≥2	
< MODERATE	119	2	POD = 23/106 = .22
≥MODERATE	83	23	FAR = 2/25 = .08

at some levels and no turbulence at others. The diagonal distribution of reports in the table suggests that breaking wave drag is very much related to turbulence intensity. The Chi-Square test statistic for dependence of the data (Conover 1971) in this table is 136.02,

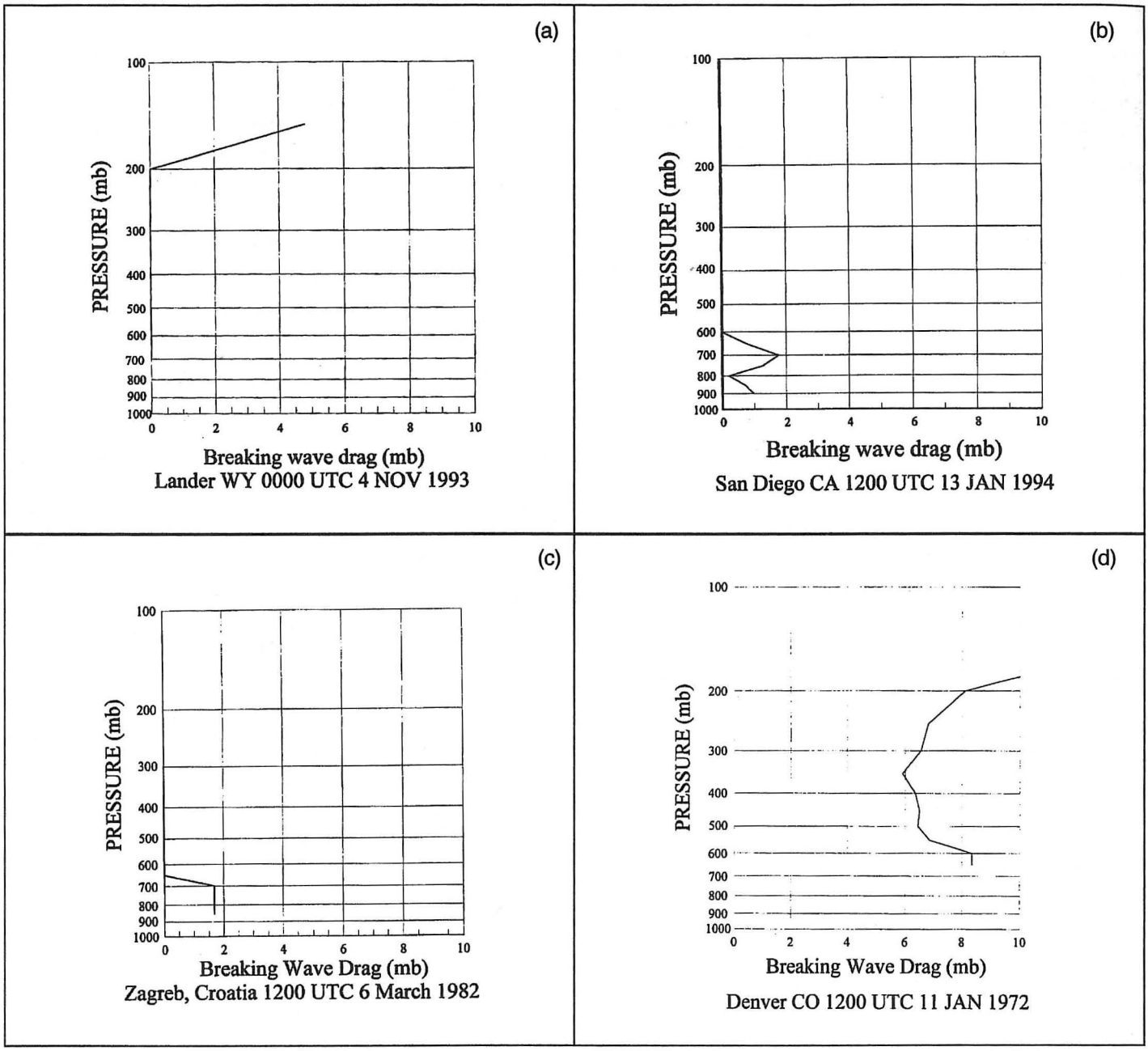

Fig. 11. Breaking wave drag profile for a) the 4 November 1993 sounding in Fig. 7, b) the 13 January 1994 sounding in Fig. 8, c) the 6 March 1982 sounding in Fig. 9, and d) the 11 January 1972 sounding in Fig. 10.

which compares with a value of 45.32 for a .999 significance with 20 degrees of freedom which confirms the relationship.

What thresholds can a forecaster use to determine when turbulence of a certain intensity will begin? The large contingency table was reduced to various 2 x 2 contingency tables to discover these thresholds. The Critical Success Index in Table 3 maximizes at higher wave drag for each increase in turbulence intensity.

In the second database, all aircraft turbulence reports located within 2 degrees of 40N 106W (near Denver, Colorado) and 34N 118W (near Los Angeles, California) were gathered from 7 December 1997 to 6 February 1998. The intensities were compared with the breaking wave drag computed from soundings interpolated from the Rapid Update Cycle numerical model to a quarter degree grid using the MWAVE algorithm (next section). Table 4 shows various 2 x 2 contingency tables for this data. Although the Probability of Detection (POD) is rather low, mountain waves are just one turbulence source, and other turbulence sources, such as boundary layer or clear air turbulence, probably account for a substantial percentage of the misses. The low False Alarm Ratio (FAR) for the various thresholds indicates that the breaking wave drag diagnostics are reliable.

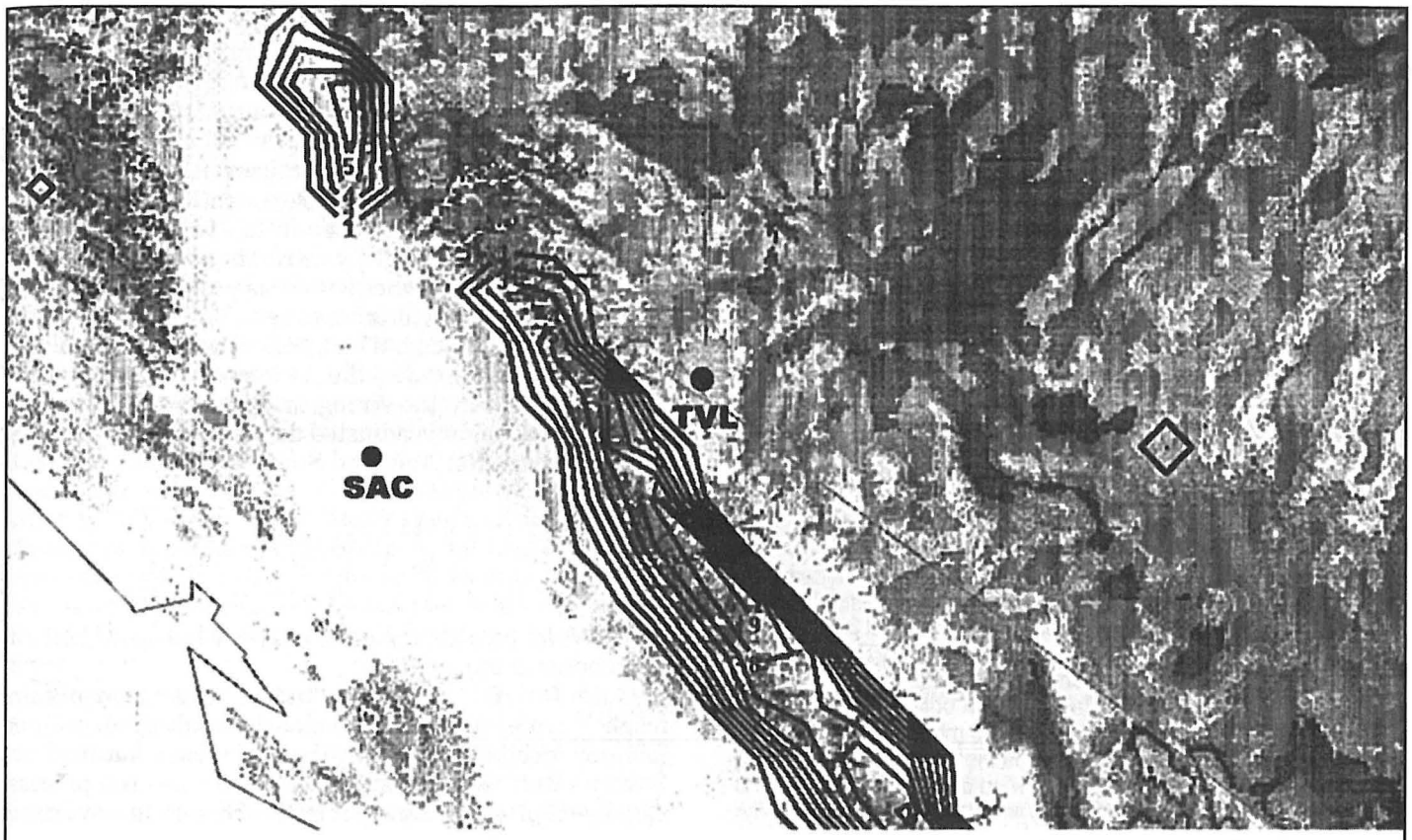

Fig. 12. MWAVE breaking wave drag diagnosis over central California from the Rapid Update Cycle (RUC) numerical model run at 2100 UTC 27 October 1996. The weather stations at Tahoe Valley (TVL) and Sacramento (SAC), both in California, are located. Units of breaking pressure drag are mb. Background map is the terrain elevation.

9. The MWAVE Algorithm

Durran (1990) expressed that a forecaster can do no better than to examine atmospheric soundings for matching characteristics with those in mountain wave breaking climatological studies. This may work for local forecasters that only need to be informed about mountain waves in their small areas of responsibility but only if a similar case has occurred in the past. Of course, someone has to create the climatoligical study for each local area. This approach works poorly since the atmospheric details causing mountain waves are sometimes different than those observed in the climatology. It is better to take the dynamical approach as outlined in Sections 2-6. Then there are the forecasters who have large areas of responsibility and must issue advisories anywhere when conditions are favorable. They need guidance in all mountainous areas, not just those that have been researched.

The MWAVE algorithm applies the wave analysis formulae to numerical model forecast data to compute breaking wave drag over any mountainous terrain. This section describes the special developmental considerations.

The mountain height, h, used in the formulae for wave breaking and wave drag assumes that the mountain is an isolated bell-shaped symmetric mountain ridge above level terrain. Since actual terrain is not ideally-shaped, the goal is to obtain a representative "mountain height" that is equivalent to the "ideal" height so one can input it into the "ideal" equations.

Section 3 outlines much of the strategy toward attaining representative mountain heights. In addition, Kim and Arakawa (1995) found that the mountain's pointedness, as measured by its concavity, also influenced the wave drag; the more upwardly-pointed the mountain, the higher the drag. Another way to visualize this effect is that narrow mountains have more wave drag than wider mountains with identical heights.

Guided by Kim and Arakawa (1995), a worldwide terrain database at 1/8 degree latitude/longitude resolution (about 12 km) provides enough elevation data to compute asymmetry and concavity. Recognizing that for any given case, the mountain top wind direction plays an important role in determining h, asymmetry and concavity were computed along both the x- and y-directions at one quarter degree resolution (about 25 km). An "asymmetry height" at any grid point, i, is defined as the negative elevation change along the positive x(y)-direction or $h_a = -(z_{i+1} - z_{i-1})$, where the subscripted z is the mean elevation along the x(y)-direction at each grid point at the one-quarter degree resolution. A "concavity height" is defined as the negative curvature along the positive x(y)-direction or $h_c = -(z_{i+1} + z_{i-1} - 2z_i)$. The simple sum ($h_a$ +

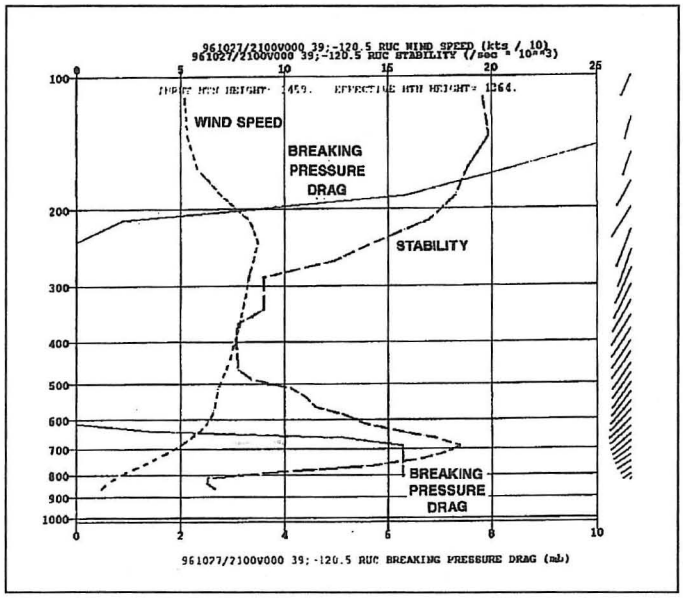

Fig. 13. Vertical profile of MWAVE input and output at 39N 120.5W at 2100 UTC 27 October 1996, the point between TVL and SAC where MWAVE breaking pressure drag was maximum. Light gray is the breaking pressure drag (abscissa on bottom). The breaking wave drag goes to zero just below the 600 mb level and returns to positive about 250 mb. Medium gray is the wind speed; dark gray is the stability (abscissa on top). The wind direction at each level is indicated in the series of vectors to the right of the profile. Wind directions are primarily northeasterly.

h_c), depending on wind direction (see below), gives very good "mountain heights." The quarter degree resolution corresponds well with a 10 km half-width mountain on which most of the mountain wave research has been based.

The results are five fixed grids of terrain statistics at one quarter degree latitude/longitude resolution. The first is a grid of the mean elevation at each grid point. There are two grids of asymmetric heights, one each in the x- and y-directions, and two similar grids of concavity heights. The terrain input grids only need to be computed once.

MWAVE produces results for the points on the fixed one quarter degree resolution grids. Therefore, the model grids need to be interpolated to the terrain grid. This is an important step for two reasons. First, the wind direction determines the asymmetry height. What is positive asymmetry for one wind direction is negative asymmetry for the opposite direction. Second, model grid resolutions vary from model to model. If MWAVE were computed on a model's grid, then the important terrain statistics would have to be computed for every model on which one wanted to run MWAVE. Furthermore, when a model's resolution changes, as they often do, one would have to recompute the terrain statistics.

Automated calculation of h on the terrain grid is a three-step process. First, the first pressure level above the sum of the terrain elevation (z_i) and the asymmetry height (h_a) becomes the "mountain top." The stability and horizontal wind in that layer are the conditions over the "mountain" at that point. Second, the mountain height, h, is computed using the following formula:

$$h = \left(h_{a_x} \frac{u}{|\mathbf{V}|} + h_{c_x} \frac{|u|}{|\mathbf{V}|} \right) + \left(h_{a_y} \frac{v}{|\mathbf{V}|} + h_{c_y} \frac{|v|}{|\mathbf{V}|} \right) \quad (5)$$

where the second subscripts indicate h_a and h_c in the x(y)-direction, $u(v)$ is the x(y)-component of the mountain top wind, and **V** is the mountain top vector wind. Note that the concavity height contribution along the x(y)-direction is the same whether $u(v)$ is positive or negative. If $h < 0$, then the height is set to zero. This formula yields large mountain "heights" slightly downwind from the actual mountain peaks, the location where mountain waves typically are the strongest.

Third, the height is adjusted downward for blocking by a formula from Rottman and Smith (1989)

$$h_{eff} = h\left(\frac{0.985}{h_0}\right) \quad h_0 = \frac{N_0 h}{U_0} > 0.985 \quad (6)$$

where N_0 is the stability and U_0 is the wind speed both at the mountain top.

Once MWAVE computes the equivalent mountain heights and interpolates the model soundings to each of its grid points, it applies the equations outlined in Sections 2 through 6. Appendix B describes the process step-by-step. MWAVE output grids of breaking wave drag in horizontal layers which, when mapped, readily show where mountain waves may cause turbulence. Figure 12 is an example in which MWAVE diagnosed high breaking wave drag from the Rapid Update Cycle model soundings over central California on 27 October 1996. There were seven pilot reports of greater than moderate turbulence in the six hours from 1800 UTC to 0000 UTC along the Tahoe Valley (TVL) - Sacramento (SAC) corridor below 12,000 feet (FL120). There were no pilot reports further to the southeast where the maximum was located. Figure 13 shows an MWAVE profile at the point along the corridor where breaking wave drag was maximized. The figure also includes profiles of wind speed and stability. Note that the 650 mb level (about FL120) was the highest level at which MWAVE had a 3 mb breaking wave drag. There were no pilot reports from above the 250 mb level to verify the positive breaking wave drag there.

10. Conclusions

Environmental stability and wind control turbulence production in mountain waves. The relationship between the two can be confusing. On the one hand, wave steepening, which measures if a wave is turbulent or not, is a function of stability divided by wind speed and is computed in all layers of a sounding. On the other hand, wave energy, which can be converted to turbulence, is a function of stability times wind speed and is computed only at the mountain top. It is constant as the wave propagates upward unless reduced by wave saturation or increased by nonlinear effects. It is a rather unique condition under which a mountain wave can produce the strongest turbulence; the winds must be strong in a stable layer at mountain top level

and diminish with height and/or stability must increase with height. Once a forecaster understands this relationship, subjectively recognizing mountain wave turbulent situations is not difficult.

However, if a forecaster must forecast aviation turbulence for large mountainous areas or if quantitative information is desired, then the sounding data must be processed. The MWAVE algorithm, described in Section 9, processes numerical model forecast soundings with the equations presented in earlier sections. To summarize, the representative mountain height, h, at a fixed terrain grid point is computed automatically from the mountain top wind direction and any diagnosed blocking. MWAVE examines wave breaking potential by calculating a local non-dimensional amplitude, considering wave saturation. Hydraulic jump-like behavior and reflection/resonance may enhance the initially computed $\hat{a}$. The wave drag in any layer is the linear drag calculated at the mountain top. Finally, MWAVE computes a breaking wave drag which is the nonlinear wave drag of breaking waves and is a measure of the turbulence intensity potential. Appendix B outlines the MWAVE process step-by-step.

What are any weaknesses of this method for diagnosing turbulent mountain waves and the MWAVE algorithm? Several years experience suggests MWAVE can be very sensitive to the observations. Input sounding data must be reasonably accurate and representative. Small errors in stability or wind speed can make large errors in a breaking drag calculation. Additionally, small differences in input mountain height can also make large differences if one of the nonlinear enhancements is important. MWAVE estimates the average mountain height in a quarter degree grid square and is thus a compromise of many factors that may not work in all instances.

Since mountain wave turbulence is not a topic taught in the typical university forecasting class, many operational meteorologists' knowledge is based on forecaster lore and fragmented information. Better forecasts should follow with the knowledge summarized in this study.

Acknowledgments

The bulk of the work for this paper was done while the author was with the Aviation Weather Center, Kansas City, Missouri. Their support, especially that of the forecast staff, was instrumental in getting this work finished. Dr. Fred Mosher's unwavering support also encouraged me to finish this work. Many readers had a hand in reviewing many versions of this paper. I appreciate all who have contributed and have made MWAVE a useful product for forecasters.

Author

Don McCann is the principal owner of McCann Aviation Weather Research, Inc. The company was founded to make available to all aviation weather forecasters the latest techniques in forecasting icing, turbulence, clouds, and convective weather. Prior to its founding, Mr. McCann was both an aviation forecaster and researcher at the National Severe Storms Forecast Center/Aviation Weather Center, Kansas City, Missouri, for 27 years. Mr. McCann has both a B.S. and an M.S. in Atmospheric Science from the University of Missouri. He has authored numerous papers on convective weather and aviation weather forecasting.

Contact information: Donald McCann, McCann Aviation Weather Research, Inc., 7306 W. 157th Terr., Overland Park KS 66223; 913-381-2209; Email: don@mccannawr.com

References

Bacmeister, J.T., P.A. Newman, B.L. Gary, and K.R. Chan, 1994: An algorithm for forecasting mountain wave-related turbulence in the stratosphere. *Wea. Forecasting*, 9, 241-253.

Blumen, W., 1990: Mountain meteorology. *Atmospheric Processes over Complex Terrain, Meteor. Monogr.*, No. 23, Amer. Meteor. Soc., 1-4.

Brinkman, W.A.R., 1974: Strong downslope winds at Boulder, Colorado. *Mon. Wea. Rev.*, 102, 592-602.

Broad, A.S., 1995: Linear theory of momentum fluxes in 3-D flows with turning of the mean wind with height. *Quart. J. Roy. Meteor. Soc.*, 121, 1891-1902.

Conover, W.J., 1971: *Practical Nonparametric Statistics*. John Wiley and Sons, New York, New York, 597 pp.

Doyle, J.D., D.R. Durran, C. Chen, B.A. Colle, M. Georgelin, V. Grusbisic, W.R. Hsu, C.Y. Huang, D. Landau, Y.L. Lin, G.S. Poulos, W. Y. Sun, D.B. Weber, M.G. Wurtele, and M. Xue, 2000: An intercomparison of model-predicted wave breaking for the 11 January 1972 Boulder windstorm. *Mon. Wea. Rev.*, 128, 901-914.

Dunkerton, T.J., 1997: Shear instability of inertia-gravity waves. *J. Atmos. Sci.*, 54, 1628-1641.

Durran, D.R., 1986: Another look at downslope windstorms, Part I: The development of analogs to supercritical flow in an infinitely deep, continuously stratified fluid. *J. Atmos. Sci.*, 43, 2527-2543.

_____, 1990: Mountain waves and downslope winds. *Atmospheric Processes over Complex Terrain, Meteor. Monogr.*, No. 23, Amer. Meteor. Soc., 59-81.

_____, and J.B. Klemp, 1983: On the effects of moisture on the Brunt- Väisälä frequency, *J. Atmos. Sci.*, 39, 2152-2158.

_____, and _____, 1987: Another look at downslope winds. Part II: Nonlinear amplification beneath wave-overturning layers. *J. Atmos. Sci.*, 44, 3402-3412.

Eliassen, A., and E. Palm, 1960: On the transfer of energy in stationary mountain waves. *Geophys. Publ.*, 22, No. 3, 23 pp.

Geller, M.A., H. Tanaka, and D.C. Fritts, 1975: Production of turbulence in the vicinity of critical levels for internal gravity waves. *J. Atmos. Sci.*, 32, 2125-2135.

Hoinka, K.P., 1984: Observations of a mountain-wave event over the Pyrenees. *Tellus*, 36A, 369-383.

_____, 1985a: A comparison of numerical simulations of hydrostatic flow over mountains with observations. *Mon. Wea. Rev.*, 113, 719-735.

_____, 1985b: Observation of the airflow over the Alps during a foehn event. *Quart. J. Roy. Meteor. Soc.*, 111, 199-224.

Kim, Y-J., and A. Arakawa, 1995: Improvement of orographic gravity wave parameterization using a mesoscale gravity wave model. *J. Atmos. Sci.*, 52, 1875-1902.

Laprise, J.R.P., 1993: An assessment of the WKBJ approximation to the vertical structure of linear mountain waves: Implications for gravity-wave drag parameterization. *J. Atmos. Sci.*, 50, 1469-1487.

Lilly, D.K., 1978: A severe downslope windstorm and aircraft turbulence event induced by a mountain wave. *J. Atmos. Sci.*, 35, 59-77.

_____, and P.J. Kennedy, 1973: Observations of a stationary mountain wave pattern and its associated momentum flux and energy dissipation. *J. Atmos. Sci.*, 30, 1135-1152.

_____, and J.B. Klemp, 1979: The effects of terrain shape on nonlinear hydrostatic mountain waves. *J. Fluid Mech.*, 45, 241-261.

McFarlane, N.A., 1987: The effect of orographically excited gravity wave drag on the general circulation of the lower stratosphere and troposphere. *J. Atmos. Sci.*, 44, 1775-1800.

Miles, J.W., and L.N. Howard, 1964: Note on a heterogeneous flow, *J. Fluid Mech.*, 20, 331-336.

_____, and H.E. Huppert, 1969: Lee waves in a stratified flow. Part 4: Perturbation approximations. *J. Fluid Mech.*, 35, 497-525.

Peltier, W.R., and T.L. Clark, 1979: The evolution and stability of finite-amplitude mountain waves. Part II: Surface drag and severe downslope winds. *J. Atmos. Sci.*, 36, 1498-1529.

Ralph, F.M., P.J. Neiman, and D. Levinson, 1997: Lidar observations of a breaking mountain wave associated with extreme turbulence. *Geophys. Res. Letters*, 24, 663-666.

Rottman, J.W., and R.B. Smith, 1989: A laboratory model of severe downslope winds. *Tellus*, 41A, 401-415.

Scorer, R.S., 1949: Theory of waves in the lee of mountains. *Quart. J. Roy. Meteor. Soc.*, 75, 41-56.

Shames, I.H., 1962: *Mechanics of Fluids*. McGraw-Hill, New York NY, 862 pp.

Shutts, G., 1995: Gravity wave drag parameterization over complex terrain: The effect of critical level absorption in directional wind shear. *Quart. J. Roy. Meteor. Soc.*, 121, 1005-1021.

Smith, R.B., 1977: The steepening of hydrostatic mountain waves. *J. Atmos. Sci.*, 34, 1634-1654.

_____, 1979: The influence of mountains on the atmosphere. *Adv. Geophys.*, 21, 87-230.

_____, 1985: On severe downslope winds. *J. Atmos. Sci.*, 42, 2597-2603.

_____, 1987: Aerial observations of the Yugoslavian bora. *J. Atmos. Sci.*, 44, 269-297.

_____, 1990: Why can't stably stratified air rise over high ground? *Atmospheric Processes over Complex Terrain. Meteor. Monogr.*, No. 23, Amer. Meteor. Soc., 105-107.

_____ and J. Sun, 1987: Generalized hydraulic solutions pertaining to severe downslope winds. *J. Atmos. Sci.*, 44, 2934-2939.

Smolarkiewicz, P.K. and R. Rotunno, 1989: Low Froude number flow past three-dimensional obstacles. Part I: Baroclinically generated lee vortices. *J. Atmos. Sci.*, 46, 1154-1164.

Weissbluth, M.J. and W.R. Cotton, 1989: Radiative and nonlinear influences on orographic gravity wave drag. *Mon. Wea. Rev.*, 117, 2518-2534.

Wurtele, M.G., 1970: Meteorological conditions surrounding the Paradise Airline crash of 1 March 1964. *J. Appl. Meteor.*, 9, 787-795.

_____, A. Datta, and R.D. Sharman, 1993: Lee waves: benign and malignant. *Proc. 5th Intl. Conf. on Aviation Weather Systems*, Amer. Meteor. Soc., Boston MA, 469.

Appendix A

A mountain wave may not be breaking ($\hat{a} > 1$) but still produce turbulence. This appendix describes why the non-dimensional amplitude threshold for positive breaking wave drag is often less than one.

Mountain waves locally modify the environmental Richardson number

$$Ri_L = \frac{\frac{g}{\Theta}\frac{d\Theta}{dz}}{\left(\frac{dN}{dz}\right)^2} \qquad \text{(A1)}$$

(g is the acceleration of gravity; Θ is the potential temperature; and $\mathbf{V}$ is the wind velocity) as described in Dunkerton (1997):

$$Ri_{mw} = Ri_E \frac{1 + \hat{a}\cos\varphi}{\left(1 + \sqrt{Ri_E}\,\hat{a}\sin\varphi\right)^2} \qquad \text{(A2)}$$

where Ri_{mw} is the mountain wave modified Richardson number and φ is the mountain wave phase angle. The transcendental functional relationship of φ indicates that the mountain wave increases and decreases the environmental Richardson number. Turbulence occurs when the modified Richardson number is less than 0.25 (Miles and Howard 1964).

Equation A2 may be evaluated whenever $\hat{a}$ and Ri_E are known. Recalling that waves break when $\hat{a} > 1$, the numerator in Eq. A2 will be less than 0.25 (actually less than zero) when $\hat{a} > 1$ for some $\pi/2 < \varphi < 3\pi/2$ ($\cos\varphi < 0$). Thus, a portion of the wave, when breaking, will be turbulent. However, the denominator in Eq. A2 may be sufficiently large even when $\hat{a} < 1$ for Ri_{mw} to be less than 0.25. The lower the Ri_E, the lower the threshold for $\hat{a}$ for turbulence production. Figure A1 shows the approximate curve.

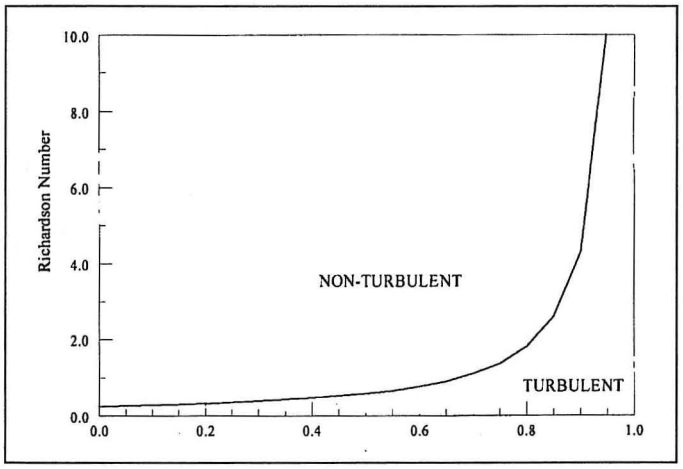

Fig. A1. Curve showing the approximate thresholds for environmental Richardson number and non-dimensional amplitude ($\hat{a} < 1$) for $Ri_{mw} < 0.25$. The curve was computed by iteratively evaluating Eq. A2.

Appendix B

This appendix describes the MWAVE process step-by-step so the readers may implement MWAVE into their forecast operations.

A preliminary task is to compute the terrain statistics needed to input into MWAVE. The National Centers for Environmental Prediction provided the 1/8 degree latitude/longitude resolution (about 12 km) global elevation database although most numerical modeling centers should have similar databases at equal or finer resolutions. Compute asymmetry and concavity "height" components along both the x- and y-directions. An asymmetry height at any grid point, i, is defined as the negative elevation change along the positive x(y)-direction or $h_a = -(z_{i+1} - z_{i-1})$, where the subscripted z is the mean elevation along the x(y)-direction at each grid point. A concavity height is defined as the negative curvature along the positive x(y)-direction or simply $hc = -(z_{i+1} + z_{i-1} - 2z_i)$. The preliminary terrain grid resolution may depend on the input database resolution. Experiments with various terrain resolutions showed problems with any resolution, but a one quarter degree resolution seemed to minimize them. This resolution corresponds with a 10 km half-width mountain on which most of the mountain wave research has been based.

1. Interpolate the model grid to terrain grid

MWAVE computes the breaking wave drag for the grid points on the fixed one quarter degree resolution grids. Therefore, the model grids need to be interpolated to the terrain grid. Interpolation algorithms are beyond the scope of this paper.

2. Compute the equivalent mountain height

Automated calculation of h on the terrain grid takes three steps. First, the first pressure level above the sum of the terrain elevation (z_i) and the asymmetry height (h_a) becomes the "mountain top level." This ensures that when the grid point is on a downslope, MWAVE uses the atmospheric conditions at the level of the nearby mountain top. The stability and horizontal wind in the layer containing the mountain top are the conditions over the "mountain" at that point.

Second, the mountain height, h, is computed using the formula

$$h = \left(h_{a_x}\frac{u}{|\mathbf{V}|} + h_{c_x}\frac{|u|}{|\mathbf{V}|}\right) + \left(h_{a_y}\frac{v}{|\mathbf{V}|} + h_{c_y}\frac{|v|}{|\mathbf{V}|}\right) \qquad \text{(B1)}$$

where the second subscripts indicate h_a and h_c in the x(y)-direction, $u(v)$ is the x(y)-component of the mountain top wind and $\mathbf{V}$ is the mountain top vector wind. When the wind changes direction with height, MWAVE computes a different mountain height for each wind direction. MWAVE uses the wind direction at the first level which the sounding height is above the ($z_i + h_a$) height. This formula yields large mountain "heights" slightly downwind from the actual mountain peaks, the location where mountain waves typically are the strongest.

Third, the height is adjusted downward for blocking by the formula

$$h_{eff} = h\left(\frac{0.985}{h_0}\right) \quad h_0 = \frac{N_0 h}{U_0} > 0.985 \qquad \text{(B2)}$$

where N_0 is the stability at the mountain top as measured by the Brunt-Väisälä frequency and U_0 is the wind speed both at the mountain top.

3. Compute wave breaking at levels above the mountain top

The non-dimensional amplitude number, $\hat{a}$, is the number which determines wave steepening,

$$\hat{a} = \frac{N_z h}{U_z}\left(\frac{N_0 U_0 \rho_0}{N_z U_z \rho_z}\right)^{1/2} \quad \text{(B3)}$$

where ρ is the air density; the zero subscripts indicate evaluation at ground level, and the z subscripts indicate evaluation in any layer aloft above sea level. This number, $\hat{a}$, indicates how the initial wave amplitude, $\hat{h}$, changes with height as it propagates upward.

One may adjust for moisture when conditions are saturated by using the saturated equivalent potential temperature instead of the potential temperature when computing N (Durran and Klemp 1983). Since N will be smaller, most saturated conditions will reduce wave breaking, but saturated conditions at the mountain top may increase h by unblocking the flow. Examine its effect on (B2). A higher h could increase the wave breaking potential aloft.

As waves steepen high enough to become turbulent, wave energy is converted to turbulent energy, and the wave energy available for turbulence production in layers aloft is reduced. Referring to Fig. 5, whenever $\hat{a}$ increases to greater than one, in layers aloft, $\hat{a}$ is reduced by the maximum $\hat{a}$ below.

To account for partial wave saturation due to the turning of the wind direction with height, the non-dimensional amplitude number is reduced by multiplying by $\cos^2(\theta z - \theta_0)$, where θ_z is the wind direction in any layer and θ_0 is the wind direction at the mountain top (Shutts 1995). If the veering or backing is greater than 90 degrees, then $\hat{a} = 0$.

4. Compute wave enhancements

Wave steepening may be enhanced in the low levels as the wave encounters conditions favorable for hydraulic jump-like behavior. MWAVE searches for a maximum in $\hat{a}$ below the highest level at which Smith's (1985) theory supports hydraulic jump-like flow. Smith (1987) gives a formule for the highest level, H_{max}, as

$$H_{\max} = \frac{U_0}{N_0}\left|h - \delta + ar\cos\left(\frac{h}{\delta}\right)\right| \quad \text{(B4)}$$

where

$$\delta = \left(\frac{\left[h^2 + h\sqrt{h^2+4}\right]}{2}\right)^{1/2} \quad \text{(B5)}$$

At all levels below the $\hat{a}_{max}$ height, $\hat{a} = \hat{a}_{max}$. This accounts for the observed turbulence between the split streamlines and assumes the turbulence in the shear layers is just as strong.

The other major influence on mountain waves is reflection and the possible resonance interaction of the reflected waves with the original wave. From Eliassen and Palm (1960) MWAVE computes a reflection coefficient

$$r = \frac{(\hat{a}_U - \hat{a}_L)^2}{(\hat{a}_U + \hat{a}_L)^2} \quad \text{(B6)}$$

where the subscripts U and L indicate evaluation at an upper and a lower level. Reflection of mountain waves will occur when there is $\hat{a}$-layering (vertical changes in $\hat{a}$), and the stronger the layering, the more the reflection, If $\hat{a}_L > \hat{a}_U$, then the reflection can lead to horizontal trapped lee waves because of the $\hat{a}$ decrease with height. If $\hat{a}_U > \hat{a}_L$, then vertical waves are reflected.

MWAVE computes a reflection/resonance enhancement with the reflection coefficient (B6). First, it computes the three-quarter vertical wavelength ($\lambda = 2\pi U_0/N_0$) height (and 1.75λ, 2.75 , ...etc., if necessary). The $\hat{a}$ computed at that level becomes the $\hat{a}_U$ in (B6). MWAVE arbitrarily uses the $\hat{a}$ at the half vertical wavelength[6] as $\hat{a}_L$. If $\hat{a}_U > \hat{a}_L$, the reflection coefficient, r, gives the fraction of the upper level wave steepening that reflects downward, $\hat{a}_{down} = r\hat{a}_U$ (Smith 1977 and Weissbluth and Cotton 1989). Since wave amplitudes add, $\hat{a}_{down}$ is added to $\hat{a}_{up}$ in layers lower than the reflecting level.

5. Compute the breaking wave drag

Linear mountain wave drag for a bell-shaped mountain with constant stability and wind aloft, D_L, is given by Miles and Huppert (1969) as

$$D_L = -\frac{\pi}{4} h\rho NU \quad \text{(B7)}$$

The linear wave drag, in any layer aloft is equal to that at the surface through the Eliassen-Palm (1960) theorem assuming no sources or sinks of wave energy exist aloft.

Nonlinear effects from wave steepening increase the wave drag. From Miles and Huppert (1969), the formula for a bell-shaped mountain is

$$D_{NL} = \left(1 + \frac{7}{16}\hat{a}^2\right) D_L \quad \text{(B8)}$$

Since it the combination of high wave breaking potential and high wave drag that is the serious problem for aviation, when $\hat{a}$ is high enough for turbulence to occur (Appendix A), the breaking wave drag (D_B) is the wave drag computed from (B8). Otherwise $D_B = 0$.

---

[6] To the author's knowledge, there are no published references on how to choose the lower level.